Article

Coplanar Electrode Layout Optimized for Increased Sensitivity for Electrical Impedance Spectroscopy

Casper Hyttel Clausen [1],*, Gustav Erik Skands [2],†, Christian Vinther Bertelsen [1],† and Winnie Edith Svendsen [1]

[1] Department of Micro- and Nanotechnology, Technical University of Denmark, Oersteds Plads 345 East, DK 2800 Kgs. Lyngby, Denmark; E-Mails: cvbe@nanotech.dtu.dk (C.V.B.); winnie.svendsen@nanotech.dtu.dk (W.E.S.)

[2] SBT Aqua ApS, Diplomvej 381, 2800 Kgs. Lyngby, Denmark; E-Mail: ges@sbtaqua.com

† These authors contributed equally to this work.

* Author to whom correspondence should be addressed; E-Mail: cahu@nanotech.dtu.dk; Tel.: +45-4525-6837; Fax: +45-4588-7762.

Abstract: This work describes an improvement in the layout of coplanar electrodes for electrical impedance spectroscopy. We have developed, fabricated, and tested an improved electrode layout, which improves the sensitivity of an impedance flow cytometry chip. The improved chip was experimentally tested and compared to a chip with a conventional electrode layout. The improved chip was able to discriminate 0.5 μm beads from 1 μm as opposed to the conventional chip. Furthermore, finite element modeling was used to simulate the improvements in electrical field density and uniformity between the electrodes of the new electrode layout. Good agreement was observed between the model and the obtained experimental results.

Keywords: electrical impedance spectroscopy; sensitivity; improved design; impedance flow cytometry

1. Introduction

Electrical impedance spectroscopy (EIS) is a relatively new technique, which has evolved from the Coulter Counter principle [1]. It probes individual particles suspended in a liquid by measuring the electrical impedance at several fixed frequencies simultaneously [2]. The multi-frequency detection allows for mapping of several properties of the sample such as size and structural composition [3,4]. The technique has been used in multiple applications within the field of flow cytometry [5], including applications that involve biological samples, such as white blood cells in different states [5] or bacteria detection and characterization [4,6,7]. Samples that have been counted and separated based on their properties include different type of white blood cells [5], living and dead yeast cells [8], as well as chemo-treated HeLa cells [4]. The technique has also been used in the monitoring of long-term cultivation micro tissue [9].

Several attempts to improve the sensitivity of the technique in order to better characterize and detect smaller particles have been made [10,11]. The simplest way to improve the sensitivity is to decrease the detection volume (smaller channel dimensions) [3], however this causes issues with respect to the particle size range that can be detected. Furthermore, the hydraulic flow resistance of the channel scales with the channel dimensions to the power of four [12]. Therefore it will become increasingly challenging [12] to efficiently pass enough sample through the microfluidic channel to obtain sufficient data recording for statistical analysis within a reasonably timespan when the channel dimensions are lowered. Other ways of optimizing the sensitivity have been done. Evander *et al.* [11] used flow focusing in their EIS device to count blood platelets and erythrocytes (red blood cells). Haandbaek *et al.* [10] did a post data bandwidth compensation technique, where they were able to differentiate between 1 and 2 μm beads in a 14×20 μm^2 channel. Further, they demonstrated that their system could distinguish 5 μm beads and yeast cells of the same size.

An alternative electrode design using front facing electrodes can also be used to increase the system sensitivity [5]. However, fabricating front facing electrodes is cumbersome and requires advanced fabrication equipment compared to the co-planar design presented in this work.

Improvements in the sensitivity of multi-frequency EIS systems, without increasing the hydraulic resistance of the channel, have great potential, as it will allow simultaneous detection and better characterization of a wider size range of particles.

The work described in this paper presents an optimized electrode layout for a microfluidic electrical impedance flow cytometer, which increases the sensitivity of the device. The advantage of this electrode layout compared to previous ones reported is that this layout achieves higher sensitivity without introducing complicated sample focusing by, e.g., dielectrophoresis/electrophoresis (DEP/EP) or flow focusing [11]. The improved layout is compared with a standard electrode layout through finite element method (FEM) and experiments. Experiments performed with the improved system demonstrated the ability of the chip to differentiate 0.5 and 1 μm beads, which was not possible for the conventional chip. The FEM was used to simulate the electrical field in the improved and conventional layout system and the simulations were compared with the obtained data to explain the results.

2. Experimental Section

2.1. Chip Design and Co-Planar Electrode Layout

A conventional EIS chip uses a differential electrode configuration, which consists of three microelectrodes at the bottom of a microfluidic channel (see Figure 1A). A voltage is applied between the center electrode (C) and the other two electrodes (A and B), while a sample of particles suspended in a liquid is continually injected through the channel. The signal is measured as a current at the ground electrodes (A and B). The signals from the outer electrodes are identical unless a particle is present between them. The signals from the two electrodes are therefore subtracted ($I_{diff} = I_{AC} - I_{BC}$) in order to baseline the signal. When a particle moves across the electrodes, the measured differential current will change depending on the type of particle and result in a characteristic transition signal. Thus, by injecting a volume of sample into the channel, the individual particles in the sample are detected and characterized one by one as they pass the electrodes.

In a conventional EIS chip, the microfluidic channel is uniform all the way through, as shown in Figure 1A. The optimized chip used in this work was designed with the same channel width as the conventional chip, except with a larger electrode area exposed to the channel as seen in Figure 1B. The limit of size detection of multi-frequency EIS is limited by the signal to noise ratio (SNR) of the chip [2]. The enlarged electrode area allows for a greater current between the electrodes and a greater current density in the constricted space between the electrodes, which is expected to lead to an improved SNR.
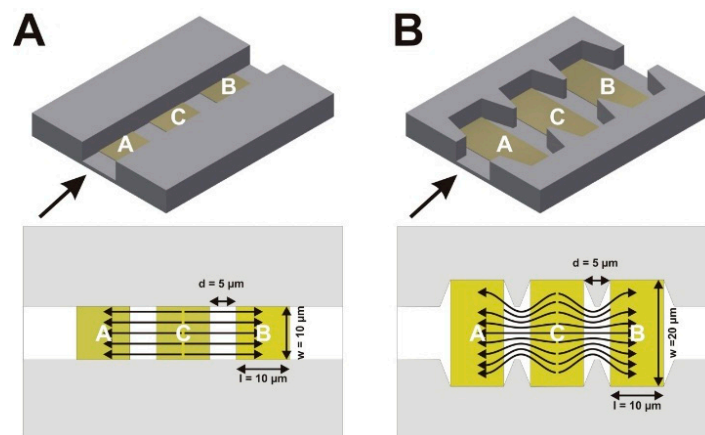
Figure 1. 3D schematic drawing of the electrode layout. (**A**) The conventional chip design. The drawing at the bottom shows the electric field between the electrodes. (**B**) The improved chip design. The drawing at the bottom shows a sketch of the electric field between the electrodes. The electric field will be denser in the constricted areas between the electrodes.

The system dimensions were chosen in order to increase the sensitivity of the chip in the sub micrometer range using standard photolithography while still being able to detect larger particles (up to 5 μm). Elongation of the electrodes along the channel direction will theoretically result in a higher current between the electrodes. However, it is not beneficial to increase the length of the electrodes significantly since this will result in inconveniently long particle transition times. The length of the electrodes was fixed at 10 μm for both the conventional and optimized design, which was found

to be a good compromise between signal strength and transition length. The distance between the electrodes was set to 5 μm (*d*) in both layouts, which provides high sensitivity while keeping a detection volume large enough for bigger particles. The chosen distance between the electrodes and electrode lengths ensures that the device is capable of single particle analysis up to a concentration of approximately 10^7 particles/mL.

The microfluidic channels in both designs are 10 μm wide and 5 μm high. The coplanar electrodes exposed to the channel in conventional chip are 10 μm wide (*w*) and 10 μm long (*l*), while for the improved chip the electrode are 20 μm wide (*w*) and 10 μm long (*l*) (see Figure 1A,B).

2.2. Finite Element Modeling

The current density was modeled by FEM simulated in COMSOL 4.3a (COMSOL AB, Kgs. Lyngby, Denmark). The selection of the dimensions of the enlargement of the area around the electrodes was based on FEM simulations. The FEM simulations were performed using the electric currents module built in to COMSOL.

2.3. Chip Fabrication and Measurement Setup

Two chip designs were fabricated for this work, one with a conventional layout (Figure 1A) and one with an optimized layout (Figure 1B).

The chips were fabricated using four inch Pyrex wafers, where 100 nm gold electrodes with a 20 nm titanium layer for adhesion were defined by a negative photolithography process (resist AZ5214e). On top of the electrodes the channels were formed in polymer (SU-8 2075 MicroChem, Berlin, Germany) by photolithography [13,14]. The chips were sealed by bonding a Pyrex lid with holes for the fluidic connections to the chips as described in [15] by applying pressure and heat. The chips were mounted in aluminum custom built holder containing fluid connections and shielded connectors for the electrical readout in order to reduce the influence of electrical noise.

2.4. Measurements

The measurements were carried out by applying an AC signal with an amplitude of 3 V (V_{peak}) and a frequency of 231 kHz to the center electrode (see Figure 2). As opposed to regular EIS measurements, only one frequency was applied since multi-frequency characterization of the sample was not necessary in order to determine the SNR properties of the chips. Changes in the AC current flowing between the electrodes, was amplified by an HF2TA current amplifier (Zurich Instruments, Zurich, Switzerland) and converted into a voltage signal and detected by an HF2IS Impedance Spectroscope (Zurich Instruments). The differential output current between the two outer electrodes was continuously recorded at a predetermined sample rate (e.g., 7200 samples/s) by a computer. A sketch of the setup is illustrated in Figure 2.

The channels were filled with phosphate buffered saline (PBS) (Sigma-Aldrich, Brøndby, Denmark) and the electrical response of the channel was characterized by frequency sweeps, prior to the experiments. As the current is detected in these experiments the frequency range of interest is where the

derivative of the Bode plot is close to zero. The resistance of the medium is dominating in this region, meaning that particles passing over the electrodes will cause maximum impedance change [3].

The experiments were carried out using 0.5, 1, and 2 μm polystyrene beads (Polysciences, Inc., Warrington, PA, USA) at a concentration of 0.5×10^6 beads/mL. The beads were suspended in PBS and injected into the chip using a Nexus 3000 syringe pump (Chemyx Inc., Stafford, TX, USA) at a rate of 0.02 μL/min. The measurements were performed with an excitation frequency of 231 kHz. At this frequency the particle dependent signal should dependent solely on the size of the particles. The sample flow was verified by inverted optical microscopy and the acquired data was analyzed using MATLAB (The MathWorks Inc., Natick, MA, USA).
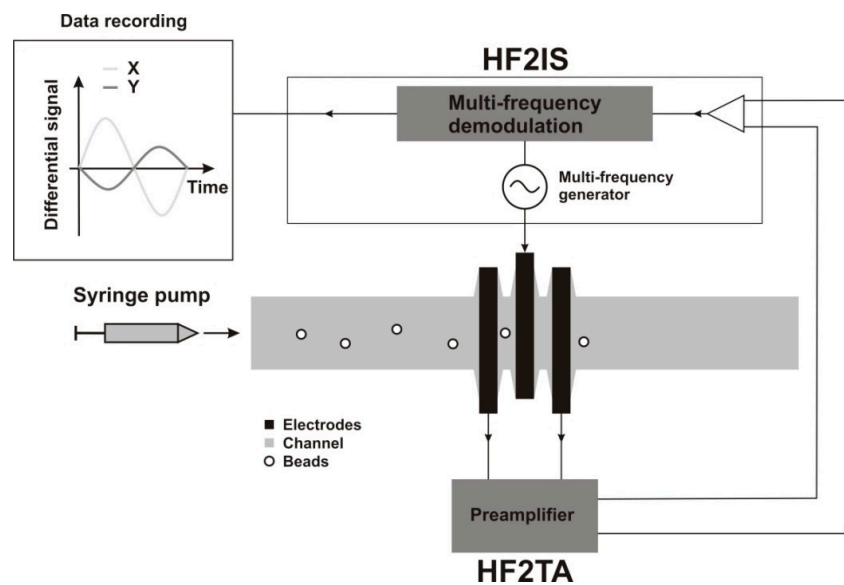

Figure 2. Schematic representation of the system. A syringe pump injects the sample into the system. The signal is generated by a multi-frequency lock-in amplifier, which also detects the signal. A current preamplifier (HF2TA, Zurich Instruments) is used to amplify the signal from the measuring electrodes before it is returned to the HF2IS Impedance Spectroscope (Zurich Instruments). A differential signal between the two measuring electrodes is recorded on a computer for further analysis by MATLAB.

3. Results and Discussion

3.1. Electrode Dimension Optimization with FEM

The optimal electrode layout and dimensions were determent using FEM simulations shown in Figure 3 based on the constrictions discussed in Section 2.1.

Three-dimensional finite element modeling in COMSOL was used to predict the magnitude and uniformity of the electric field between the electrodes when varying their width. This was done by evaluating the normalized current density through a cut plane in the narrow area between the electrodes as indicated in red on Figure 3A. A 3 V potential at 231 kHz was applied to the central excitation electrode while the two outer measurement electrodes were defined as ground (0 V). The medium between the electrodes was defined as water with a conductivity of 1.6 S/m and a relative permittivity of 80.
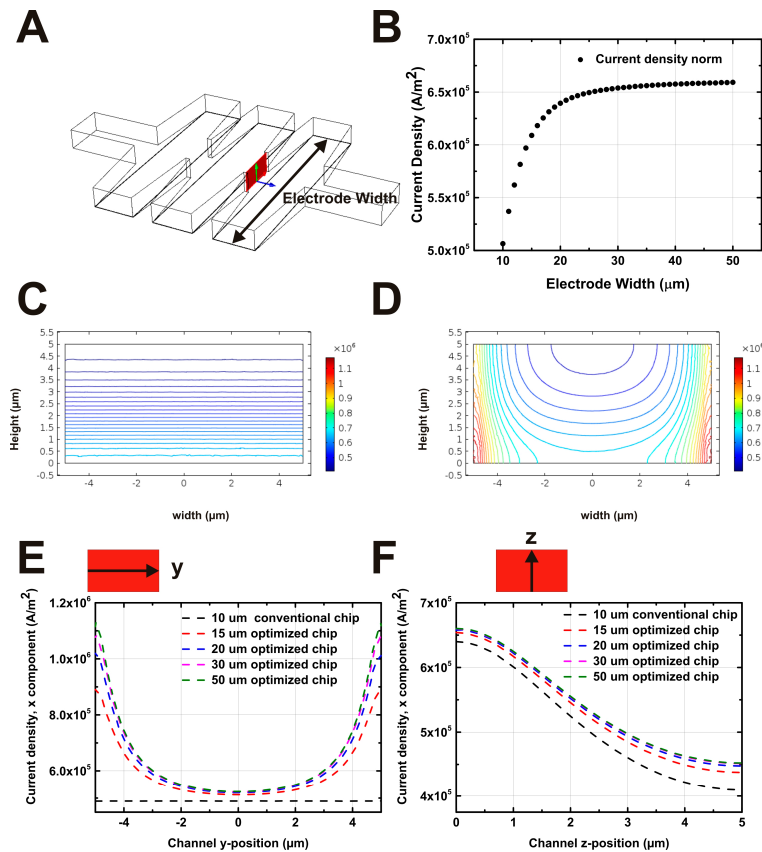
Figure 3. FEM simulation of the current density. (**A**) 3D sketch of the channel with wide electrodes. The current density was evaluated through the detection cross-section (red surface) between the electrodes using FEM. (**B**) Normalized current density through the detection cross-section as a function of electrode length the optimized chip. (**C**) Contour plot of the current density in the detection cross-section for the conventional electrode layout. (**D**) Contour plot of the current density in the detection cross-section for the improved electrode layout. (**E**) Line plot of the *x*-component of the current density for *z* = 2.5 μm as a function of the *y*-coordinate across the detection cross section for varying electrode widths. (**F**) Line plot of the *x*-component of the current density for *y* = 0 μm as a function of the *z*-coordinate across the detection cross-section for varying electrode widths.

The current density through the cross-sectional cut-plane was evaluated by surface integration for channels with electrode widths ranging from 10 μm (flush with the channel wall) to 50 μm (Figure 3B). The simulation predicts that the current between the electrodes will saturate when the electrode width is in the order of 20 μm, indicating that the design of the chip will not gain any more sensitivity from increasing the width beyond this point. While a larger current is expected to result in better sensor sensitivity it is not necessarily beneficial to extent the electrode width beyond 20 μm. The key disadvantage of widening the electrodes relates to the fluid dynamic properties of the channel. A significant enlargement of the electrode area can give rise to problems with turbulent flow around the edges of the enlargement; which is highly undesirable in a system relying on detection of transitions. Furthermore, issues can arise with the flow in the enlarged channel regions where particle trapping can occur due to areas with dead flow. However, particle trapping was not observed during experiments with the channel layout proposed in this paper.

Figure 3C,D show the contour plots of the electric current density through the cross-sectional detection plane for the original design with an electrode width of 10 μm and the improved design with an electrode width of 20 μm. It is seen that the current density varies more for the channel with the improved layout compared to the channel with the original layout; however the overall current density is 68% higher in the improved channel. The larger current density of the optimized chip should allow for higher signal and thus better SNR.

The current density across the detection cross-section in the *y*- and *z*-directions for different electrode widths is plotted in Figure 3E,F. An electrode width of 10 μm corresponds to a conventional, straight channel. The variation of current density in the *z*-direction is not influenced much by the enlargement of the electrode width, while in the y-direction there is a significant increase near the channel wall when the electrode is widened. As the flow rate used in this these experiment are sufficiently low, we do not expect that the particles will be influenced by inertial forces from the liquid, which means that the *z*- and *y*-position of the particle during the transition will be random. Some will transition near the edge and some in the center of the channel. It is therefore expected that while the improved electrode layout will provide an overall higher SNR it will also lead to a larger spread in measured current.

3.2. Chip Characterization

Figure 4A,B shows the impedance characterization of a single set of electrodes from 200 kHz to 10 MHz, of both the conventional and improved chips. The shape of the curves follows the typical trend for a fluidic channel [3].
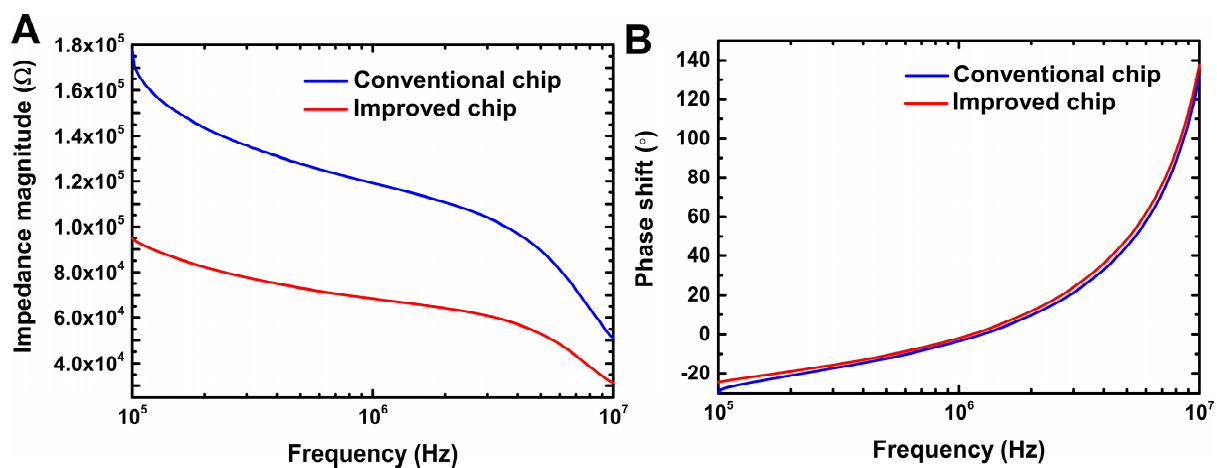
Figure 4. Frequency sweep of chips used for the experimental work. (**A**) Impedance magnitude as a function of frequency for the conventional and improved chips. (**B**) Phase shift/angle as a function of frequency for the conventional and improved chips.

The frequency dependant characterization of the impedance magnitude is plotted in Figure 4A for the conventional and improved chips. The impedance is seen to be higher in the conventional chip compared to the improved chip, meaning that the current is larger between the electrodes in the improved design, which is in accordance with the FEM simulations. The frequency dependent phase angle is plotted in Figure 4B and follows the expected trend for the channel design [3]. The small discrepancy is expected to be due to variations in the fabrication of the two chips.

Figure 5A shows the time dependant noise level of the two different electrode layouts. The root mean square of the noise from the different signals are with an *n* value of 2000, conventional real = 2.4585×10^{-10} A, conventional imaginary = 1.90681×10^{-10} A, optimized real = 2.9216×10^{-10} A, and optimized imaginary = 4.1071×10^{-10} A. Figure 5B–F show single transitions of the different detected particles for the two systems. It is seen that the shape of the time dependant transition is slightly elongated and more defined in the optimized chip design due to the different geometrical layout of the channel and electrodes. This is due to the lower flow velocity in the enlarged regions of the channel and the concentrated electric field in the constricted area between the electrodes, respectively.
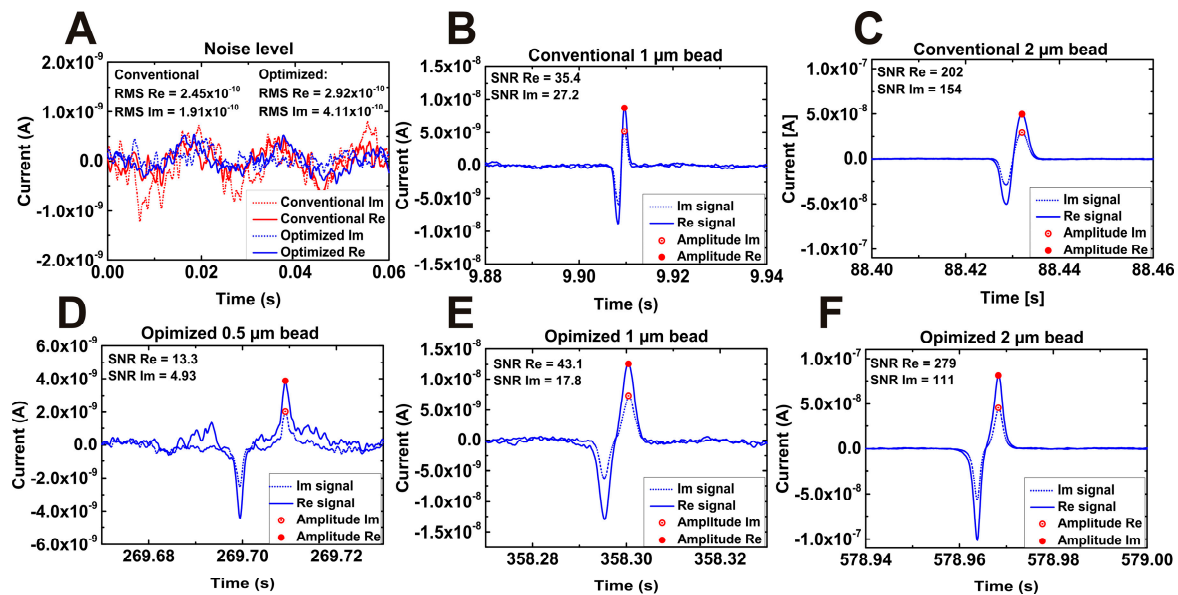

Figure 5. Signal plots in time of the transitions of the different particles in the conventional and optimized chip design. (**A**) Plot of the noise level of the different chip systems. (**B**) 1 μm bead in the conventional chip. (**C**) 2 μm bead in the conventional chip. (**D**) 0.5 μm bead in the optimized chip. (**E**) 1 μm bead in the optimized chip. (**F**) 2 μm bead in the optimized chip.

Figure 6 shows a histogram of the current response of samples with polystyrene beads with a diameter of 2 μm and samples of mixed polystyrene beads with diameters of 0.5, 1, and 2 μm, while they pass the electrodes in the conventional chip (green and red) and improved chip (blue and magenta) with an excitation signal on the center electrode of 3 V AC at 231 kHz.

As can be seen in Figure 6, the data obtain from the conventional chip yields a well-defined distribution of 2 μm beads (green) with a peak around 60 nA. It is also seen that the mixed beads sample injected through the conventional chip (red) split into two distinct distributions; one with a peak around 60 nA, and one with a peak closer to 10 nA. Since one of the populations coincides with the distribution of 2 μm beads it is assumed the beads with diameters of 0.5 μm and 1 μm make up the population at the low end of the current spectrum. It is also possible, however, that the 0.5 μm beads are not detected at all. Based on this, it is concluded that it is not possible to differentiate between polystyrene beads with diameters of 0.5 μm and 1 μm using the conventional electrode design. The histogram distributions of the recorded current response from the optimized chip (blue and magenta) are also shown in Figure 5. For the optimized chip it is seen that the mixed beads sample (magenta)

split into three distributions indicating the system's ability resolve 0.5, 1, and 2 μm beads. The two histograms also show, as expected from the FEM simulations, that the current response from identical particles is larger for the improved chip. Further, the larger spread of the 2 μm beads in the histogram from the improved chip arise either from the larger variation in the current density or comes from the chip's better size resolution. This is in agreement with the simulations shown in Figure 3. The analysis of the distributions seen in Figure 6 is shown in Table 1. The measured current is expected to scale linearly with particle volume. This means that the current is expected to increase by a factor of eight when moving from beads with a radius 0.5 μm to beads with a radius of 1 μm and, similarly, another factor of eight when moving from a radius of 1 μm to a radius of 2 μm. However, the values in Table 1 do not support this assumption. It is seen that the mean, median and mode for the analyzed population scale with a factor of five to seven when the radius of the detected beads is doubled. Since the measurements were performed on mixed samples (*i.e.*, the measurement on all bead sizes were performed under identical conditions) for both chip designs, it is very unlikely that this discrepancy is due to measurement error. It is speculated that this is due to the vertical variation of the electric field in the conventional chip and the vertical and horizontal variation in the optimized chip.
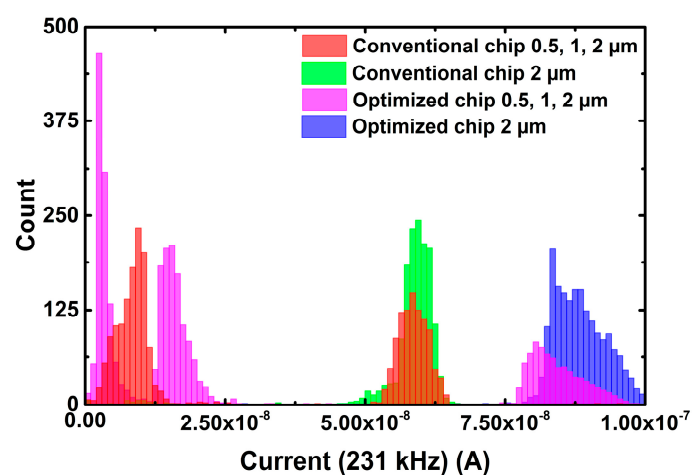
Figure 6. Histogram of the maximum current response of samples with beads with a diameter of 2 μm for the optimized (blue) and conventional (green) chip designs and samples with mixed beads with diameters of 0.5, 1, and 2 μm for the optimized (magenta) and conventional (red).

Table 1. Calculated mean, median, mode and standard deviation of the two populations obtained from the measurements of the mixed sample in the conventional chip (red) and the three populations obtained from the measurements of the mixed sample in the optimized chip (magenta) shown in Figure 6.

Electrode layout	Sample	Mean (nA)	Median (nA)	Mode (nA)	Standard deviation (nA)
Conventional	Mixed—2 μm PS beads (red)	58.8	58.5	58	3.8
Conventional	Mixed—1 μm PS beads (red)	8.4	8.5	10	3.1
Optimized	Mixed—2 μm PS beads (magenta)	84.3	83.3	81	6.3
Optimized	Mixed—1 μm PS beads (magenta)	16.4	15.7	15	3.6
Optimized	Mixed—0.5 μm PS beads (magenta)	3.4	3.0	3	1.4

In comparison with the FEM simulations it seen that the improved sensitivity of the system corresponds well with what is expected.

4. Conclusions

In conclusion, we have designed, fabricated, and tested an improved coplanar electrode layout for use in electrical impedance spectroscopy. The optimization of the chip layout was carried out using FEM simulation. Improved chips were tested using beads and were successful in discriminating beads with 0.5, 1, and 2 μm diameters. The developed chip is a huge improvement when compared to the conventional coplanar electrode layout of the same dimension, which was only capable of discriminating beads above 1 μm. Further, the finite element method was used to verify the increased sensitivity by mapping the increase in current density.

Acknowledgments

Author Contributions

Performing of the experiments, analysis of the data, and theoretical modeling were carried out by Casper Hyttel Clausen, Christian Vinther Bertelsen and Gustav Erik Skands. Chip design was done by Casper Hyttel Clausen. Chip fabrication was carried out by Gustav Erik Skands. FEM simulations were carried out by Christian Vinther Bertelsen. All authors contributed to the design of the experiments and the drafting of the manuscript.

Supplementary Materials

Supplementary materials can be accessed at: http://www.mdpi.com/2072-666X/6/1/110/s1.

Conflicts of Interest

The authors declare no conflict of interest.

References

1. Coulter, W.H. Means for Counting Particles Suspended in a Fluid. U.S. Patent 2,656,508, 20 October 1953.
2. Gawad, S.; Schild, L.; Renaud, P.H. Micromachined impedance spectroscopy flow cytometer for cell analysis and particle sizing. *Lab Chip* **2001**, *1*, 76–82.
3. Morgan, H.; Sun, T.; Holmes, D.; Gawad, S.; Green, N.G. Single cell dielectric spectroscopy. *J. Phys. D Appl. Phys.* **2007**, *40*, 61–70.
4. Kirkegaard, J.; Clausen, C.; Rodriguez-Trujillo, R.; Svendsen, W. Study of Paclitaxel-Treated HeLa Cells by Differential Electrical Impedance Flow Cytometry. *Biosensors* **2014**, *4*, 257–272.

5. Holmes, D.; Pettigrew, D.; Reccius, C.H.; Gwyer, J.D.; van Berkel, C.; Holloway, J.; Davies, D.E.; Morgan, H. Leukocyte analysis and differentiation using high speed microfluidic single cell impedance cytometry. *Lab Chip* **2009**, *9*, 2881–2889.

6. Haandbaek, N.; With, O.; Burgel, S.C.; Heer, F.; Hierlemann, A. Resonance-enhanced microfluidic impedance cytometer for detection of single bacteria. *Lab Chip* **2014**, *14*, 3313–3324.

7. David, F.; Hebeisen, M.; Schade, G.; Franco-Lara, E.; Di Berardino, M. Viability and membrane potential analysis of Bacillus megaterium cells by impedance flow cytometry. *Biotechnol. Bioeng.* **2012**, *109*, 483–492.

8. Mernier, G.; Hasenkamp, W.; Piacentini, N.; Renaud, P. Multiple-frequency impedance measurements in continuous flow for automated evaluation of yeast cell lysis. *Sens. Actuator B Chem.* **2012**, *170*, 2–6.

9. Schumacher, Z.; Frey, O.; Hierlemann, A. Microfluidic impedance spectroscopy scanner for spherical microtissues. In Proceedings of 15th International Conference on Miniaturized Systems for Chemistry and Life Sciences, Seattle, WA, USA, 2–6 October 2011,

10. Haandbaek, N.; Mathwig, K.; Streichan, R.; Goedecke, N.; Bürgel, S.C.; Heer, F.; Hierlemann, A. Bandwidth Compensation for High Resolution Impedance Spectroscopy. *Procedia Eng.* **2011**, *25*, 1209–1212.

11. Evander, M.; Ricco, A.J.; Morser, J.; Kovacs, G.T.A.; Leung, L.L.K.; Giovangrandi, L. Microfluidic impedance cytometer for platelet analysis. *Lab Chip* **2013**, *13*, 722–729.

12. Bruus, H. *Theoretical Microfluidics*; Oxford University Press: New York, NY, USA, 2008.

13. Demierre, N.; Braschler, T.; Linderholm, P.; Seger, U.; van Lintel, H.; Renaud, P. Characterization and optimization of liquid electrodes for lateral dielectrophoresis. *Lab Chip* **2007**, *7*, 355–365.

14. Moresco, J.; Clausen, C.H.; Svendsen, W. Improved anti-stiction coating of SU-8 molds. *Sens. Actuator B Chem.* **2010**, *145*, 698–701.

15. Serra, S.; Schneider, A.; Malecki, K. A simple bonding process of SU-8 to glass to seal a microfuidic device. In Proceedings of 3rd International Conference on Multi-Material Micro Manufacture, Borovets, Bulgaria, 3–5 October 2007.